Nanoscale

PAPER

View Article Online
View Journal | View Issue

Cite this: *Nanoscale*, 2026, **18**, 10795

A novel manganese glycerophosphate vaccine gel elicits broad and durable immunity across an aged and pox virus model

Md Jahirul Islam,†[a] Luis Ontiveros-Padilla,†[a] Stephen A. Ehrenzeller,†[a] Denzel D. Middleton,[a] John A. Roque, III,[a] Connor T. Murphy,[a] Nicole Rose Lukesh,[a] Dylan A. Hendy,[a] Erik S. Pena,[a,b] Ryan N. Stack,[c] William J. Polacheck,[c] Eric M. Bachelder[a] and Kristy M. Ainslie *[a,b,d]

Subunit vaccines, composed of a protein antigen and an adjuvant, offer a safer and more versatile strategy than traditional live-attenuated vaccines, but limitations of conventional adjuvants like alum require improved design and delivery. Manganese (Mn) has emerged as a novel adjuvant that stimulates the cGAS-STING pathway, showing profound pre-clinical efficacy in vaccines against infectious diseases and cancer, but its potential dose-limiting toxicities require innovative delivery strategies. Herein, we report the development of gel derived from the generally recognized as safe (GRAS) material manganese glycerophosphate (MnGp). The gel displayed tunable controlled antigen release based on MnGp concentration that activated dendritic cells (DCs) *in vitro*, eliciting substantial production of type I interferons and upregulation of costimulatory markers. A single immunization of mice with ovalbumin (OVA) and 250 mg mL^{-1} MnGp gel generated the highest and most durable OVA-specific total IgG, IgG1, and IgG2c serum antibody titers. Subsequently, a prime-boost-boost immunization with 250 mg mL^{-1} MnGp gel elicited a long-lasting OVA-specific IgG, IgG1, and IgG2c sera antibody response and it was superior to MF59-mimic AddaVax and STING agonists 2,3-cGAMP. Splenocytes from mice immunized with MnGp secreted high levels of Th1-associated cytokines upon antigen recall and illustrated generation of memory $CD4^+$ and $CD8^+$ T cells. Immunizing MnGp in 18-month-old mice elicited superior IgG and IgG1 antibody titers compared to Addavax, in addition to specific T cell responses in spleen and the draining lymph node. Finally, the co-immunization of MnGp and B5R (a vaccinia virus protein) induced higher B5R-specific antibody titers than Addavax and achieved full protection against the challenge with vaccinia virus. Overall, these findings corroborate the potential for MnGp gels as a novel vaccine platform.

Received 17th September 2025,
Accepted 27th March 2026

DOI: 10.1039/d5nr03936c

rsc.li/nanoscale

Introduction

Vaccination stands as one of the most successful public health measures to date with the worldwide eradication of Smallpox in 1980 as a shining example of this effort.[1,2] Smallpox, caused by *Variola major* and *V. minor*, is responsible of the death of an estimated 10% of the human population over thousands of years, including 300–500 million deaths in the 20th century alone. Despite its eradication, smallpox remains a critical bioterrorism threat, and outbreaks of related *Orthopoxviruses* (*e.g.*, monkeypox (mPox)) continue to pose public health risks due to zoonotic transmission.[3,4] In November 2022, the WHO reported over 78 000 cases of monkeypox with more than 98% occurring in non-endemic regions. This unprecedented spread prompted the WHO to declare the outbreak a Public Health Emergency of International Concern.[5,6] In response to the outbreak, the Bavarian-Nordic vaccine, JYNNEOS, was distributed to those deemed at high-risk for mPox exposure. JYNNEOS received an Emergency Use Authorization (EUA) by the FDA, which allowed for intradermal administration and subsequent dose-sparing. While this significantly slowed the spread of disease, the protection elicited by the JYNNEOS vaccine has been shown to quickly wane, as the vaccine generates suboptimal quantities of neutralizing antibodies.[7] JYNNEOS also contains a live-attenuated, non-replicating vaccinia virus, which is considerably safer than the replication-competent

[a]*Division of Pharmacoengineering and Molecular Pharmaceutics, Eshelman School of Pharmacy, University of North Carolina at Chapel Hill, Chapel Hill, North Carolina, USA. E-mail: ainsliek@email.unc.edu*
[b]*Joint Department of Biomedical Engineering, University of North Carolina at Chapel Hill and North Carolina State University, Chapel Hill, North Carolina, USA*
[c]*Lampe Joint Department of Biomedical Engineering, University of North Carolina at Chapel Hill and North Carolina State University, Chapel Hill, North Carolina, USA*
[d]*Department of Microbiology & Immunology, UNC School of Medicine, University of North Carolina at Chapel Hill, Chapel Hill, North Carolina, USA*
†Authors contributed equally.

strain used in the older ACAM2000 vaccine. However, some safety concerns remain, particularly for immunocompromised populations.[8]

With the available mPox vaccines, a broad vaccination strategy for the general public would be limited since it does not take into consideration high-risk individuals, such as those who are living with HIV and would have compromised immunity.[9,10] Vaccine development to protect high-risk populations is gaining attention recently due to the SARS-CoV-2 mRNA vaccine, which demonstrated profound efficacy in preventing severe illness and improving disease outcomes in aged, immunocompromised, and high-risk comorbidity populations.[11–13] Nevertheless, complications observed with the mRNA vaccine rollout and global distribution (*e.g.* poor stability outside of cold-chain storage) and carrier-mediated reactogenicity,[14,15] highlight the continual need to develop novel vaccine formulations for high-risk populations.

Traditional vaccine development is largely focused on the production of live attenuated pathogens, but the capacity for vaccine strains to replicate in and cause illness to the host prompts safety concerns for immunocompromised populations.[16,17] In contrast, subunit vaccines, composed of purified proteins, peptides, or polysaccharides from a pathogen, are noninfectious and offer a promising alternative that avoids these safety concerns.[18] Because subunit antigens are weakly immunogenic and typically induce only modest humoral responses with little to no cellular immunity, subunit vaccines often include adjuvants to enhance and sustain the immune response.[19] Aluminum-containing adjuvants (*i.e.*, alum) are perhaps the most widely used subunit vaccine adjuvants, largely due to their potency, safety profile, and relatively accessible cost.[20] However, despite proven efficacy in several licensed vaccines, alum primarily elicits a T helper 2 (Th2) cell-biased response (*i.e.*, antibody-mediated, or humoral immunity) with a marginal T helper 1 (Th1) cell response (*i.e.*, cell-mediated immunity).[21] Thus, for diseases where a robust Th1 response is critical, such as influenza and certain cancers,[22,23] candidate vaccines require more effective adjuvant systems. As such, significant progress has been made in the exploration of depot-forming emulsion systems like MF59, adjuvant system 01 (AS01) and AS03.[24–26] Further, there is a greater development for agonist which stimulate pattern recognition receptors such as toll-like receptor (TLR) agonists (*e.g.*, poly(I:C), CpG), and cyclic GMP-AMP synthase (cGAS)-stimulator of interferon genes (STING) agonists (*e.g.*, cGAMP) to invoke a Th1 vaccine responses.[27–29]

Manganese (Mn) is an emerging adjuvant that possesses varied effects on the cGAS-STING pathway.[30–33] Classically, the cGAS-STING pathway orchestrates the immunological responses to double-stranded DNA (dsDNA). Upon binding dsDNA, cGAS catalyzes the synthesis of the second messenger cyclic GMP-AMP (cGAMP), which subsequently binds and activates STING. Activated STING then initiates a number of downstream processes, ultimately resulting in the expression of type I interferons and several interferon-stimulated genes that regulate the anti-viral immune response.[34] Interestingly, Mn(II) has been found to augment cGAS-STING through both DNA-dependent and DNA-independent mechanisms. Manganese was first discovered to modulate the sensitivity of cGAS-STING to dsDNA, as Mn-deficient WT mice demonstrated increased susceptibility to dsDNA, but not RNA, viruses in a STING-dependent manner.[31] Alternatively, manganese has since been shown to directly activate cGAS to synthesize cGAMP,[33] as well as to associate with cGAMP to enhance cGAMP-STING binding affinity.[31] Given these mechanisms, several groups have already investigated the adjuvanticity of manganese to augment anti-tumor and anti-viral responses with substantial success.[30,35]

To enhance delivery of manganese to target immune cells, these adjuvants have largely been encapsulated in or formulated as nanoparticles.[36–41] Although improved compared to soluble injections of Mn, many of these formulation strategies require sophisticated fabrication processes that are poorly scalable. Furthermore, nanoparticles often offer limited antigen/adjuvant dosing and are rapidly cleared from the injection site. In contrast, gel-based delivery systems offer several potential advantages that address the limitations of nanoparticle-based formulations. Foremost, many gel-like formulations exhibit shear thinning behavior, characteristic of pseudoplastic or thixotropic materials, which allows them to form a well-defined and long-lasting depot upon injection. Given that several adjuvant systems, including nanoparticles, exploit this phenomenon to prolong immune responses,[42] developing a gel-based formulation for manganese could further enhance antigen and adjuvant retention and controlled release at the injection site, while also acting as a cGAS-STING agonist to potentially elicit a stronger and more sustained immune response. Furthermore, depending on the chemistries, gels can be highly scalable, thermostable, and optimized for a wider range of administration profiles (*e.g.*, mucosal, intradermal).[43] Therefore, a gel-based formulation for Mn-adjuvanted vaccines represents a promising yet underexplored strategy to improve vaccination.

Herein, we report the fabrication and characterization of a novel gel derived from manganese glycerophosphate (MnGp), hereafter referred to as an MnGp gel. The US FDA recognizes manganese glycerophosphate as a generally regarded as safe (GRAS) material, underscoring the potential safety of our gel formulation. Compared to typical polymeric initiators used in the fabrication of gel-based drug delivery formulations, MnGp was selected as the gel precursor as it bypasses the need for adjuvant encapsulation or chemical ligation, thereby circumventing a potentially limiting design consideration and instilling the delivery system with inherent adjuvanticity. Following the development of a facile and scalable fabrication method, MnGp gels were first assessed for antigen release kinetics and *in vitro* activation of relevant immune cell populations at a range of concentrations. Subsequently, we evaluated the potential for MnGp to act as vaccine platforms *in vivo*. We characterized the dosing, immunization schedules, humoral and cellular immunity and the protection induced by this platform against the *Orthopoxvirus* vaccinia. Finally, we immunized

MnGp in an aged mice model to assessed the immune response induced by this vaccine in a high-risk group of vaccination.

Methods

Materials

Unless otherwise specified, all chemicals were purchased and used unmodified from Sigma Aldrich (St Louis, MO) and all assays, biologics, and disposables were purchased from ThermoFisher Scientific (Waltham, MA). Separately, commercial adjuvants (Addavax, CpG, cGAMP) were acquired from Invivogen (San Diego, CA).

Preparation and characterization of MnGp gels

A dry mixture of MnGp (Pfaltz & Bauer; Waterbury, CT) and sucrose was resuspended to 350 mg mL^{-1} MnGp and 150 mg mL^{-1} sucrose in 0.1M HEPES. The suspension was then placed in an ice bath and probe sonicated (Q500 Sonicator; QSonica Sonicators; Newtown, CT) for 30 minutes (1 second on, 1 second off) at maximum amplitude (100%). After sonication, the resultant gel was stored at 4 °C until use. Endotoxin level was confirmed to be less than 0.1 EU/dose using a limulus amoebocyte lysate-based assay.

MnGp gels were imaged using scanning electron microscopy (SEM; Hitachi S-4700 Cold Cathode Field Emission; Ibaraki, Japan; UNC CHANL). To prepare samples, a droplet of the MnGp gel was spread on an SEM sample mount affixed with adhesive carbon tape. The mount was then submerged in liquid nitrogen for 1 minute and lyophilized for at least 48 hours prior to imaging.

The viscosity characterization of Mn-Gp gels was performed using Discovery HR-20 rheometer (TA Instruments) with a 20 mm diameter parallel plate geometry (100–110 μm). A frequency sweep test was performed at 20° C with shear rate ranging from 0.0001 to 1000 (1 s^{-1}) using logarithmic sampling (5 points per decades). Shear thinning behavior was quantified using the Ostwald–de Waele power-law model, expressed in viscosity from as:

$$\eta = K\left(\frac{du}{dy}\right)^{n-1}.$$

Assessment of OVA release from MnGp gels

5, 25, 100 and 250 mg mL^{-1} MnGp gels were prepared *via* dilution of the stock 350 mg mL^{-1} MnGp gel in 0.1 M HEPES and subsequently loaded with OVA protein (Fisher Scientific; New Hampton, NH) *via* mixing. To measure OVA release from the MnGp gels, 50 μL of the OVA-loaded MnGp gels were dispensed into 96-well plates and layered with 200 μL PBS, with three wells prepared for each timepoint. At each timepoint, the plates were centrifuged at 500*g* for 5 minutes, and the supernatant was collected and stored at 4 °C prior to analysis. OVA content in the supernatant was quantified using a Bradford's assay following the manufacturer's protocol. Percent release was quantified as the amount of OVA present in the supernatant relative to the known OVA content initially loaded in each gel aliquot.

Cell culture and treatments

All experiments involving mice were performed with the approval of the University of North Carolina at Chapel Hill Institutional Animal Care and Use Committee (IACUC). Bone marrow-derived dendritic cells (BMDCs) were differentiated from murine bone marrow as previously described.[44–46] In short, C57BL/6J mice (Jackson Laboratory; Bar Harbor, ME) were humanely euthanized and bone marrow was collected from the femurs and tibias. The bone marrow-derived cells were then cultured in Roswell Park Memorial Institute 1640 medium (RPMI 1640; Corning; Corning, NY) supplemented with 10% heat-inactivated fetal bovine serum (FBS; Corning), 1% penicillin–streptomycin solution (Corning), and 10 ng mL^{-1} GM-CSF for 10 days, followed by RPMI 1640 supplemented with 10% heat-inactivated FBS, 1% penicillin–streptomycin solution, 10 ng mL^{-1} GM-CSF, and 10 ng mL^{-1} IL-4 for the next 4 days. After the 14 day culture, cells were immediately used for cell-based assays.

To assess the immunostimulatory properties of the MnGp gel, BMDCs were cultured with the MnGp gel in a transwell model. The bottom of a 12-well transwell plate was first precoated with the 100 mg mL^{-1} MnGp gel, and BMDCs were then plated at 1×10^5 cells per well in the upper transwell insert. Additional BMDCs were cultured in base media with and without 100 ng mL^{-1} LPS. To determine changes in cell phenotype, cells were collected after 12 hours and stained with eBioscience Fixable Viability Dye (eFluor 506; Fisher Scientific; New Hampton, NH) and the following fluorophore-conjugated antibodies (Biolegend; San Diego, CA): MHC-II (FITC, clone: M5/114.15.2), CD86 (PE, clone: GL-1), CD80 (PE/Cy7, clone: 16-10A1), CD40 (APC/Cy7, clone: 3/23), CD11c (BV421, clone: N418), and CD11b (BV711, clone: M1/70). To determine cytokine secretion levels, cell supernatants were collected after 24 hours and the concentration of IFN-β was determined *via* ELISA (R & D Systems; Minneapolis, MN).

In vivo immunizations & sample collection

For the initial MnGp gel titration studies, 6–8 week-old C57BL/6J mice (n = 5 per group) were immunized intramuscularly on day 0 with saline, soluble OVA (25 μg per mouse), OVA + AddaVax, OVA + 5 mg mL^{-1} MnGp gel, OVA + 25 mg mL^{-1} MnGp gel, OVA + 100 mg mL^{-1} MnGp gel, or OVA + 250 mg mL^{-1} MnGp gel. Mice were dosed at 25 μL per hind limb (50 μL total) and 25 μg of endotoxin-free OVA (Invivogen; San Diego, CA). AddaVax formulations were prepared *via* 1 : 1 v/v mixing of AddaVax (Invivogen) with OVA according to the manufacturer's protocol. MnGp gel formulations were prepared as described for the OVA release studies. Submandibular bleeds were subsequently collected biweekly through week 18 (day 126).

For subsequent immunization studies, 6–8 weeks old C57BL/6J mice (n = 5) were immunized intramuscularly on

days 0, 28 and 140 with saline, soluble OVA (25 μg per mouse), OVA + AddaVax, OVA + 2,3-cGAMP (1 μg), OVA + 250 mg mL^{-1} MnGp, or OVA + 250 mg mL^{-1} MnGp + 2,3′-cGAMP (0.01, 0.1, or 1 μg). Mice were boosted on day 140 to stimulate cellular responses. Submandibular bleeds were collected biweekly through week 18 (day 126), as well as 10 days following the final boost (day 150). On day 151, mice were humanely euthanized to collect spleens and draining lymph nodes (dLNs), which were subsequently processed into single cell suspensions as previously described.[47]

For the aged mice study, 18 month-old C57BL/6J mice (n = 5) were obtained from the National of Institute of Aging and were immunized intramuscularly on days 0 and 28 as described above with PBS, OVA (25 μg per mouse), 250 mg mL^{-1} MnGp + OVA (1 : 1 v/v and 25 μg) or Addavax + OVA (1 : 1 v/v and 25 μg). Submandibular bleeds were collected biweekly and on day 77 mice were homologous boosted to evaluate the cellular immune response. On day 84, spleens were harvested and processed into single cell suspensions as previously described.

Challenge study

6–8 week-old BALB/c mice (n = 10) were immunized intramuscularly on days 0 and 28 as described above with PBS, CpG + B5R (10 μg each item per mouse), 250 mg mL^{-1} MnGp + B5R (1 : 1 v/v and 10 μg) or Addavax + B5R (1 : 1 v/v and 10 μg). Submandibular bleeds were collected biweekly until day 56 when each mouse was challenged intranasally with 5×10^4 pfu of vaccinia virus (Western Reserve – NR-55). Survival and weight loss were monitored for 14 days after challenge. Mice were also scored according to previous studies,[48] based on the presentation of the next clinical signs: 0 (normal), 1 (slightly ruffled fur), 2 (clearly ruffled fur), 3 (hunched posture and/or conjunctivitis with fur ruffling), and 4 (score of 3 combined with difficulty breathing/moving/socializing).

Determination of antibody titers

OVA-specific and B5R-specific antibody titers in the collected sera were determined by a previously described indirect ELISA method.[44,49] Briefly, high-binding 384-well plates (Greiner Bio-One; Kremsmünster, Austria) were coated with OVA (10 μg mL^{-1}) or B5R (1 μg mL^{-1}) in PBS and incubated at 4 °C overnight. Plates were then blocked with 3% w/v instant nonfat dry milk in PBS (blocking buffer; Food Lion; Salisbury NC) for 1 hour at room temperature (RT) and incubated with sera samples across a range of dilutions for 2 hours at RT. Plates were subsequently incubated with IgG, IgG1, and IgG2c-specific HRP-conjugated detection antibodies (Southern Biotech; Birmingham AL) for 30 minutes at RT. 3,3,5,5-Tetramethylbenzidine (TMB) was then added to initiate the detection reaction, and development was quenched with 2 N sulfuric acid. A minimum of three washes with 0.05% v/v Tween 20 in PBS (PBST) were performed between each step. Absorbances at 450 and 570 nm were read on a plate reader (SpectraMax M2 Microplate Reader; Molecular Devices; Sunnyvale, CA), with the 570 nm absorbance subtracted from the 450 nm absorbance to correct for background. Titer was determined using a plot of correct absorbance against serum dilution factor as previously reported.[50,51]

Assessment of antigen recall

Antigen recall was assessed by both ELISA and ELISPOT, as previously described.[44,47,49,50] For ELISAs, splenocytes and dLN cells from immunized mice were plated at 1×10^6 cells per well in a 96-well plate and incubated with 10 μg mL^{-1} OVA protein for 36 hours. After 36 hours, the cell supernatants were collected and stored at −80 °C until use. IFN-γ, IL-4 and IL-2 content in the supernatants was measured *via* ELISA according to the manufacturer's protocol (Biolegend; San Diego, CA). For ELISPOTs, splenocytes from immunized mice were plated at 1×10^6 cells per well in a multi-screen-IP 0.45 μm filter 96-well plate (Sigma Aldrich; St. Louis, MO) pre-coated with the desired capture antibody. Cells were then incubated with 10 μg mL^{-1} OVA protein for 36 hours, and ELISPOTs were developed according to the manufacturer's protocol (BD Biosciences; San Jose, CA). Spots were counted with the AID Classic ELISpot Reader (AID Autoimmun Diagnostika GmbH; Straßberg, Germany).

Immune cell phenotyping *via* flow cytometry

Following generation of single cell suspensions from spleens, cells were stained to assess immune phenotype and OVA-specificity. To profile immune cell phenotypes, 1×10^6 cells were stained with eBioscience Fixable Viability Dye (eFluor 506) and the following fluorophore-conjugated antibodies (Biolegend; San Diego, CA): CD3 (AF488, clone: 17A2), CD4 (APC/Fire 750, clone: RM4-5), CD8 (PerCP/Cy5.5, clone: 53-6.7), CD44 (BV421, clone: IM7), CD62L (BV785, clone: MEL-14), CD19 (APC, clone: 6D5), GL7 (PE, clone: GL7), and CD38 (PE/Cy7, clone: 90). Tetramer staining to assess OVA-specificity was performed as a separate panel. In short, 1×10^6 cells were first incubated with 50 nM desatinib for 30 minutes at 37 °C. Cells were subsequently stained with OVA Class I (AF568, clone: H2-Kb/SIINFEKL), OVA Class II (BV421, clone: I-A(b)/AAHAEINEA), or control tetramers (clone: I-A(b)/PVSKMMRMATPLLMQA) acquired from the NIH Tetramer Facility at Emory University (Atlanta, GA). Cells were then stained with the following fluorophore-conjugated antibodies (Biolegend; San Diego, CA): CD3 (AF488, clone: 17A2), CD4 (APC/Fire 750, clone: RM4-5), and CD8 (PerCP/Cy5.5, clone: 53-6.7). Following staining, cells were fixed with 1% paraformaldehyde and analyzed with an Attune NxT flow cytometer (ThermoFisher Scientific; Waltham, MA; UNC Flow Core Facility). Analysis of flow data was performed with FlowJo v10.9.0.

Statistical analysis

Figures and statistical analyses were prepared with GraphPad Prism 10. For *in vitro* adjuvanticity experiments, all data were compared *via* ordinary one-way ANOVA with Tukey's multiple comparisons test. For *in vivo* kinetics of vaccination studies, in order to compare the data between groups and the different

time points, all data were compared *via* ordinary two-way ANOVA with Tukey's multiple comparisons test.

Results & discussion

Synthesis and characterization of the MnGp gel

Sonication has been previously reported to develop metallogel and hydrogel platforms,[52–54] where pulsatile forces, local temperature changes, and aeration are hypothesized to facilitate cross-linking of the gel-forming reagents. We hypothesized that the sustained high-intensity sonication of a concentrated solution of MnGp would promote gelation *via* hydrogen bonding. More specifically, mechanical disruption of the MnGp salts in an aqueous environment likely forces hydration of the salts and/or salt aggregates, thereby coordinating MnGp molecules *via* shared hydrogen bonding with intercalating water molecules.[55] Additionally, we opted to incorporate sucrose into the formulation due to its known properties as both a gel stabilizer and cryoprotectant.[56]

In this case, we were able to successfully synthesize a MnGp gel *via* probe sonication on ice for 30 minutes (Fig. 1A). Comparison of the gel mixture before and after sonication demonstrated a significant shift in fluidity and viscosity, as evidenced by the retention of MnGp gel at the top of an inverted scintillation vial (Fig. 1B). SEM of a lyophilized MnGp gel revealed an irregular architecture with microporous layers. The structure showed two different pore sizes: small pores of around 5–15 μm (approximately 30% of the total pores) and medium size pores of around 20–40 μm (approximately 70% of the total pores). All this data suggests that there could be significant fluid retention in the gel matrix (Fig. 1C).

Interestingly, the same architecture was observed for MnGp gels prepared without sucrose (Fig. S1), suggesting that interactions between manganese glycerophosphate and water are the primary cross-linking mechanisms. For the same reason, its degradation is expected to occur primarily through ionic exchange and coordination bond dissociation under physiological conditions.

Given the application of many gel-like materials as controlled release formulations, release of the model antigen OVA was measured from MnGp gels under physiological conditions (37 °C, pH 7.4). OVA-loaded MnGp gels were prepared at various concentrations post-sonication by dilution of the stock

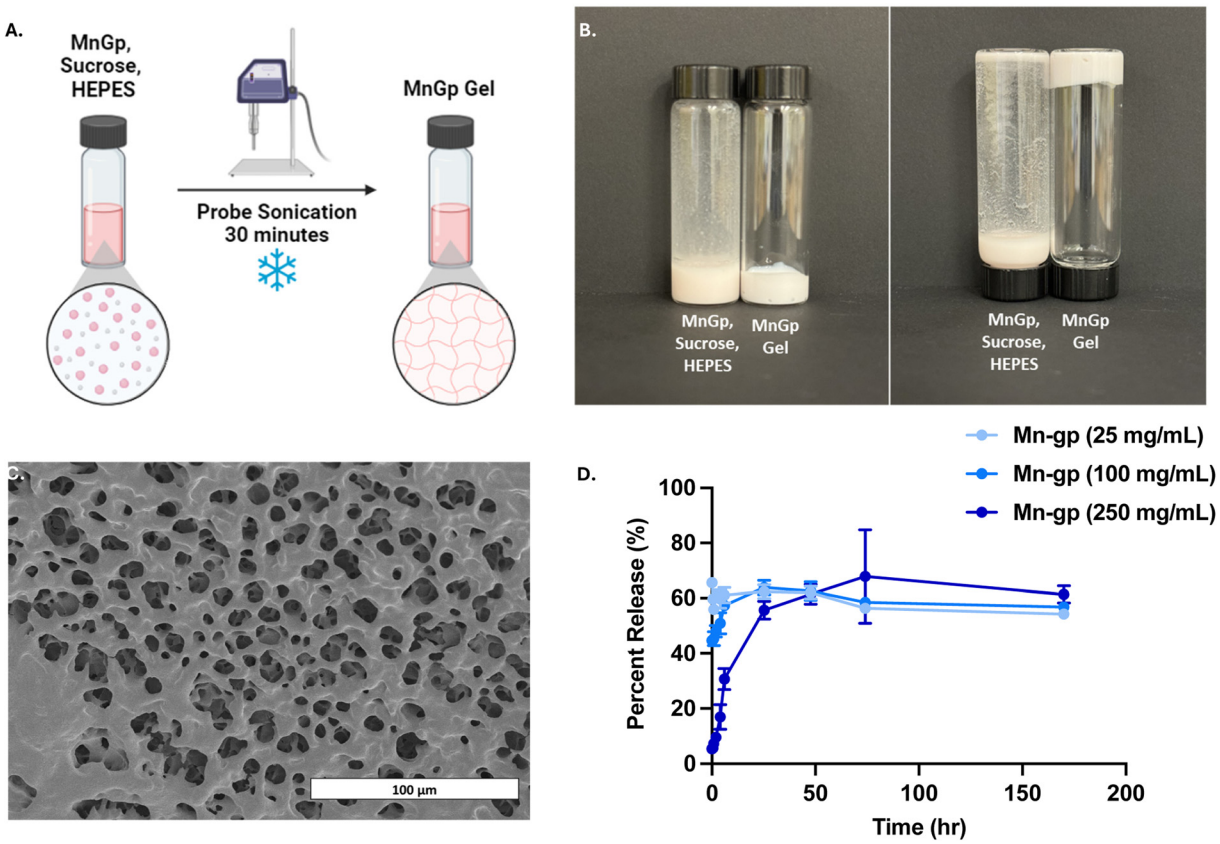

Fig. 1 Synthesis and characterization of MnGp gel. (A) Synthesis schematic of MnGp gel. A concentrated solution of MnGp (350 mg mL^{-1}) and sucrose (150 mg mL^{-1}) in 0.1 M HEPES was probe sonicated for 30 minutes on ice, yielding the MnGp gel. (B) Comparison of the pre-sonication gel mixture (left) and resultant gel (right), with inverted containers documented to demonstrate fluidity and viscosity changes. (C) Scanning electron microscopy (SEM) image of the stock MnGp gel. (D) OVA-release by MnGp gels at various MnGp concentrations. The stock MnGp gel (350 mg mL^{-1} MnGp) was diluted to the indicated concentrations in 0.1M HEPES and loaded with OVA *via* vortexting. Release was monitored over 1 week at physiological conditions (pH 7.4, 37 °C) and measured *via* Bradford's assay. Data is presented as mean ± standard deviation (n = 3).

gel in 0.1 M HEPES and simple mixing with OVA. The generated OVA release curves indicated clear concentration-dependent kinetics (Fig. 1D). The 250 mg mL^{-1} MnGp gel had the slowest release, exhibiting a low burst release (around 5–10% percent of OVA) and approximately 60% of OVA released by 48 hours. The 100 mg mL^{-1} MnGp gel demonstrated slightly slowed kinetics, although burst release was nearly 50% and total release leveled off at around 60% OVA release after 24 hours. Both the 25 and 5 mg mL^{-1} MnGp gels exhibited no control over OVA release. These release kinetics aligned strongly with SEM of these gels, with increasing porosity and dispersity observed with decreasing concentration of MnGp. In addition, SEM analysis revealed concentration-dependent microstructural transitions in the gels. Lower MnGp concentrations produced highly porous microporous networks, consistent with lower cross-linking interactions and larger mesh size. Increasing MnGp concentration resulted in more compact and homogeneous architectures, while intermediate concentrations displayed fibrillar structures, suggesting diffusion-limited aggregation during gel formation (Fig. S2A–C). The SEM of the OVA-loaded gel showed a change in the gel structure (Fig. S3), suggesting that some OVA protein might only interact on the surface, although according to our release studies, the majority of the protein is loaded inside the gel.

Notably, no gels fully released their cargo, indicating that some OVA might be sequestered within the gel and inaccessible to facile diffusion out of the gel matrix. It is important to note that *in vivo* release kinetics have not been performed yet and it could be an important experiment to completely understand the behavior of this formulation. When analyzing the rheological properties of the MnGp gel, we identified a shear thinning behavior, given the decrease in viscosity as the shear rate increased and a value of the power-law index (n) of less than 1 (Fig. S4). This is a highly desired characteristic for adjuvant gels because enables it to be injected as a low viscosity, flowing material and to form a stable long-lasting depot upon injection.[57,58]

In vitro adjuvanticity of the MnGp gel

To determine the immunostimulatory properties of the MnGp gel, BMDCs were cultured with the 100 mg mL^{-1} MnGp gel and assessed for relevant phenotypic changes and cytokine secretions (Fig. 2A–D). As DCs are the primary innate immune cell population involved in T cell education and activation, the response of DCs to the MnGp gel provides an early insight into the potential efficacy of a vaccine platform. After 12 hours, the MnGp gel was well tolerated, with slight reductions in cell viability observed compared to the untreated (UT) and LPS controls (Fig. 2A); which can be explained, as in previous reports, due to increased levels of cleaved-caspase 3 detected in cells stimulated with STING activators.[59] MnGp gel treatment led to a marked upregulation of co-stimulatory molecules, with a significant increase in the frequency of $CD80^{+}CD86^{+}$ cells (Fig. 2B), and more than a twofold rise in the median fluorescence intensities (MFI) of CD80 (Fig. S5A) and CD86 (Fig. S5B) compared to untreated cells. Furthermore, treatment with the MnGp gel resulted in a considerable increase in MHC-II MFI (Fig. 2C). Given that MHC-II is one of the molecules by which DCs present antigens to T cells, and both CD80 and CD86 are co-stimulatory molecules involved in T cell activation, these data suggest that the MnGp gel aptly poises DCs for presentation of antigen to T cells. Additionally, after 24 hours, there were significantly elevated levels of IFN-β in the cell supernatants of MnGp gel-treated cells compared to the untreated and LPS controls (Fig. 2D), consistent with previous reports of manganese stimulating the cGAS-STING pathway.[32] Type I interferons such as IFN-β are also associated with improved T cell activation and differentiation into Th1-like phenotypes.[60] In the present study, IFN-β production was used as a functional downstream readout of pathway activation. Although upstream signaling intermediates (*e.g.*, cGAS activation, STING translocation, TBK1/IRF3 phosphorylation) were not directly assessed, the increased IFN-β levels are consistent with activation of the canonical STING signaling cascade. However, this *in vitro* data further underscores the potential of the MnGp gel as a vaccine platform *in vivo.*

In vivo titration of OVA-loaded MnGp gel vaccine

Initial dose titration studies were performed to identify the optimal MnGp gel concentration for use as a vaccine platform. Mice were immunized once with saline, unadjuvanted OVA, OVA + AddaVax (analogous to FDA-approved adjuvant MF59), or OVA-loaded MnGp gels of increasing MnGp concentration, and sera were collected biweekly to measure OVA-specific IgG titers (Fig. 3A–C). Total IgG titers exhibited concentration-dependent responses; wherein higher MnGp gel concentrations elicited superior titers (Fig. 3A). Across all adjuvanted groups, total IgG titers peaked around 70 days post-immunization and subsequently decreased, with the 250 mg mL^{-1} MnGp gel inducing the highest and most sustained titers. It is reasonable that these results are due in part to concentration of manganese at the injection site, as well as the increased viscosity of the higher concentration MnGp gels since the same volume of gel was injected. The 250 mg mL^{-1} MnGp gel forms a well-defined, long-lasting depot in the intramuscular space, likely resulting in continued recruitment and activation of innate immune cells such as dendritic cells. IgG1 and IgG2c were additionally measured as markers of Th2 and Th1 responses, respectively.[61,62] Both IgG1 (Fig. 3B) and IgG2c (Fig. 3C) titers mirrored the trends observed for total IgG, albeit at lower levels. Notably, the 100 and 250 mg mL^{-1} MnGp gels elicited significantly higher IgG2c titers compared to OVA adjuvanted with AddaVax at peak titers, suggesting that the MnGp gels might offer a more efficacious platform for inducing Th1 responses. Based on these data, 250 mg mL^{-1} MnGp was identified as the optimal formulation for further studies.

Humoral response to optimal OVA-loaded MnGp gel vaccine

Initial concentration titration studies evaluated the durability of the humoral response following a single vaccination with OVA-loaded MnGp gel formulations. However, many vaccines often utilize sequential immunization, or boosts, to bolster

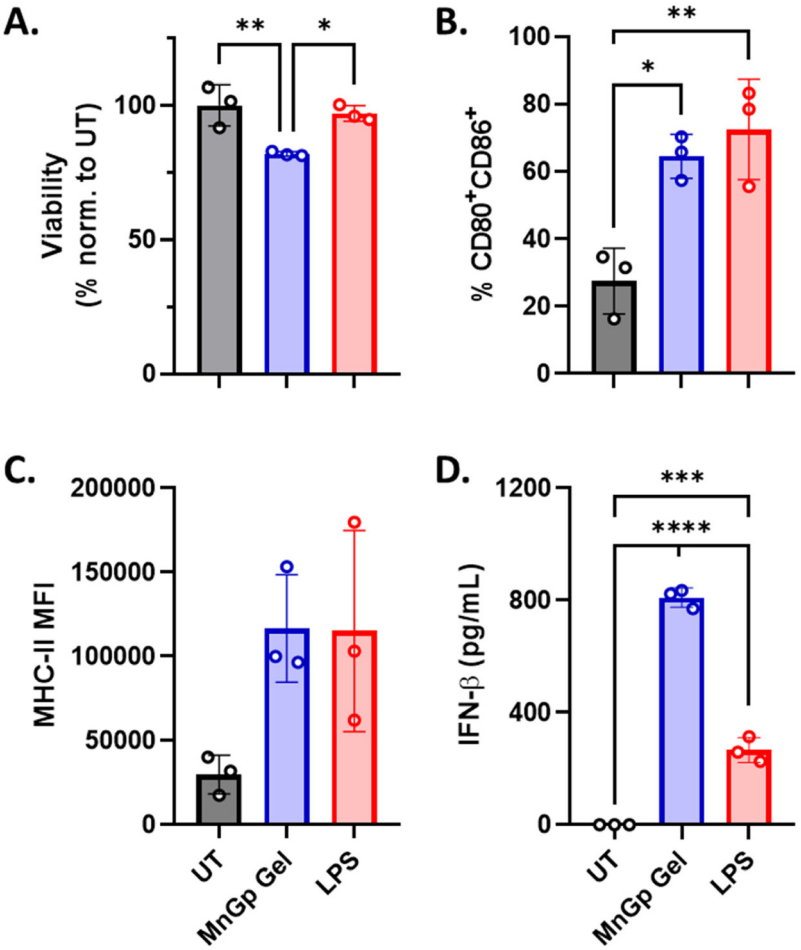

Fig. 2 Activation of BMDCs by MnGp gel. BMDCs were cultured with media (UT), the 100 mg mL^{-1} MnGp gel, or 100 ng mL^{-1} LPS. (A) Normalized cell viability, (B) frequency of $CD80^+CD86^+$ cells, and (C) median fluorescence intensity (MFI) of MHC-II was assessed after 12 hours *via* flow cytometry. (D) IFN-β concentrations in the cell supernatants after 24 hours were measured *via* ELISA. Data is presented as mean ± standard deviation (n = 3). Statistical significance is presented as *p < 0.05, **p < 0.01, ***p < 0.001, and ****p < 0.0001 for an ordinary one-way ANOVA with Tukey's multiple comparisons test.

immune memory and ensure long-term protection. Therefore, we sought to better characterize the immune response to the MnGp gel with a prime-boost schedule. Mice were immunized on days 0 and 28 with saline, unadjuvanted OVA, OVA + AddaVax, OVA + 250 mg mL^{-1} MnGp gel, or OVA + 2,3 cGAMP (an established STING agonist). An additional boost was performed on day 140 for subsequent cellular analyses. Also, given the ability of manganese to augment the cGAS-STING pathway, the 250 mg mL^{-1} MnGp gel was co-loaded with OVA and various doses of cGAMP to assess potential synergy.

As before, sera were collected biweekly and assessed for OVA-specific IgG titers (Fig. 4A–C). Compared to a single immunization (Fig. 3), boosting 28 days after the initial immunization yielded notably higher overall total IgG, IgG1, and IgG2c (Fig. 4A–C) titers at subsequent timepoints. Titer kinetics additionally followed the same trend as with the prime-only vaccination, with titers initially peaking around day 70 and gradually decreasing thereafter for all IgG subtypes. Although trend was the same, the magnitude of response was significant with IgG and IgG1 titers remaining on average around 10^6, which is notably high in this model. This long-lasting and significant antibody response represents a desired characteristic given that the usual antibody kinetics is to start decreasing 2 weeks post-boost.[63] Following a second boost on day 140, titers rapidly returned to their peak levels (Fig. 4A–C). Consistent with the single immunization titers, the 250 mg mL^{-1} MnGp gel outperformed the AddaVax-adjuvanted cohort, with boosting resulting in significantly higher total IgG, IgG1, and IgG2c (Fig. 4A–C) titers throughout most of the time course. Similarly, the 250 mg mL^{-1} MnGp gel elicited significantly higher titers across all measured subtypes compared to the cGAMP-adjuvanted cohort (Fig. 4A–C). Thus, when compared to both another depot-forming adjuvant system (MF59) and cGAS-STING-targeting adjuvant (cGAMP), the MnGp gel demonstrates significant promise in humoral immunity alone. The addition of cGAMP did not significantly increase the humoral response, across a range of cGAMP doses (Fig. S6), suggesting that MnGp might saturates local cGAS-STING sig-

naling. Consequently, mice immunized with the MnGp-cGAMP combination were not included in the subsequent analysis.

Cellular response to optimal OVA-Loaded MnGp gel vaccine

Cellular responses to vaccines are critical for durable protection, control of reinfection, and defense against pathogens when antibodies are insufficient. In addition to the humoral response and their neutralizing activity, the protection against smallpox acquired by vaccination has been linked to cellular immunity, primarily through $CD4^+$ and $CD8^+$ T cells. Those virus-specific T cells are responsible for clearing the initial infection, with robust memory populations persisting for decades and controlling the early stages of the infection.[64,65] Thus, we sought to profile the specific immune phenotypes associated with sequential immunization with the MnGp gel vaccine formulation.

After the antigen recall of splenocytes, at day 151 and after following a prime-boost-boost immunization schedule on days 0, 28, and 140; a trend of high IL-2-producing-cells and significant higher number of IFN-γ-secreting cells (Fig. 5A and B) were observed in mice of the MnGp vaccinated cohort compared to all other cohorts. A similar result was observed, with significantly higher levels of IL-2 and IFN-γ from splenocytes

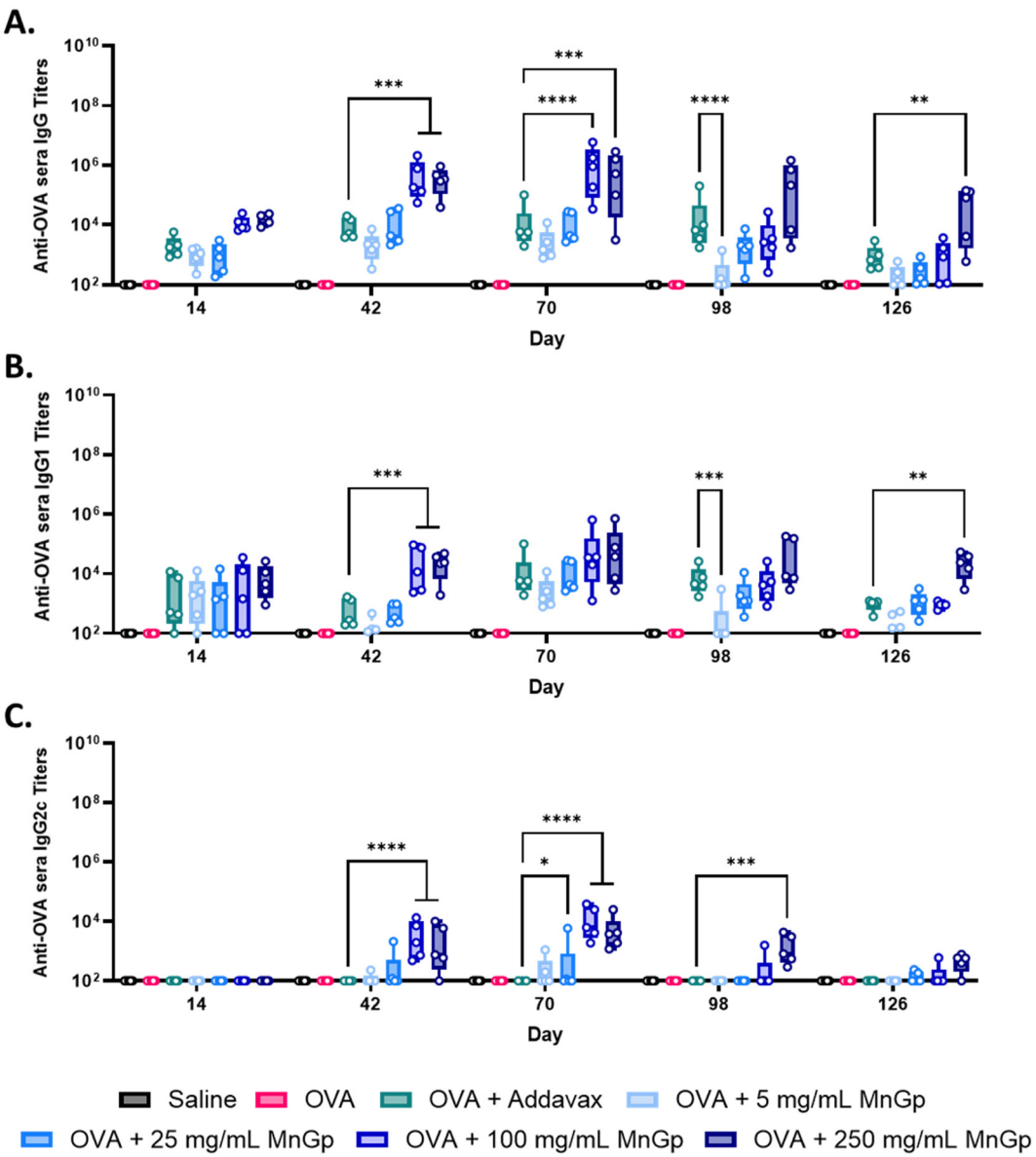

Fig. 3 OVA-specific serum antibody titers following a single immunization. C57BL/6 mice (n = 5) were immunized intramuscularly on day 0 with saline, unadjuvanted OVA, OVA + Addavax, or OVA + the indicated concentrations of the MnGp gel. Sera were collected at the indicated timepoints and assessed for OVA-specific (A) total IgG, (B) IgG1, and (C) IgG2c titers *via* ELISA. Data is presented as median ± range. Statistical significance is presented as *p < 0.05, **p < 0.01, ***p < 0.001, and ****p < 0.0001 for an ordinary two-way ANOVA with Tukey's multiple comparisons test. Absence of statistical symbols indicates non-significant differences.

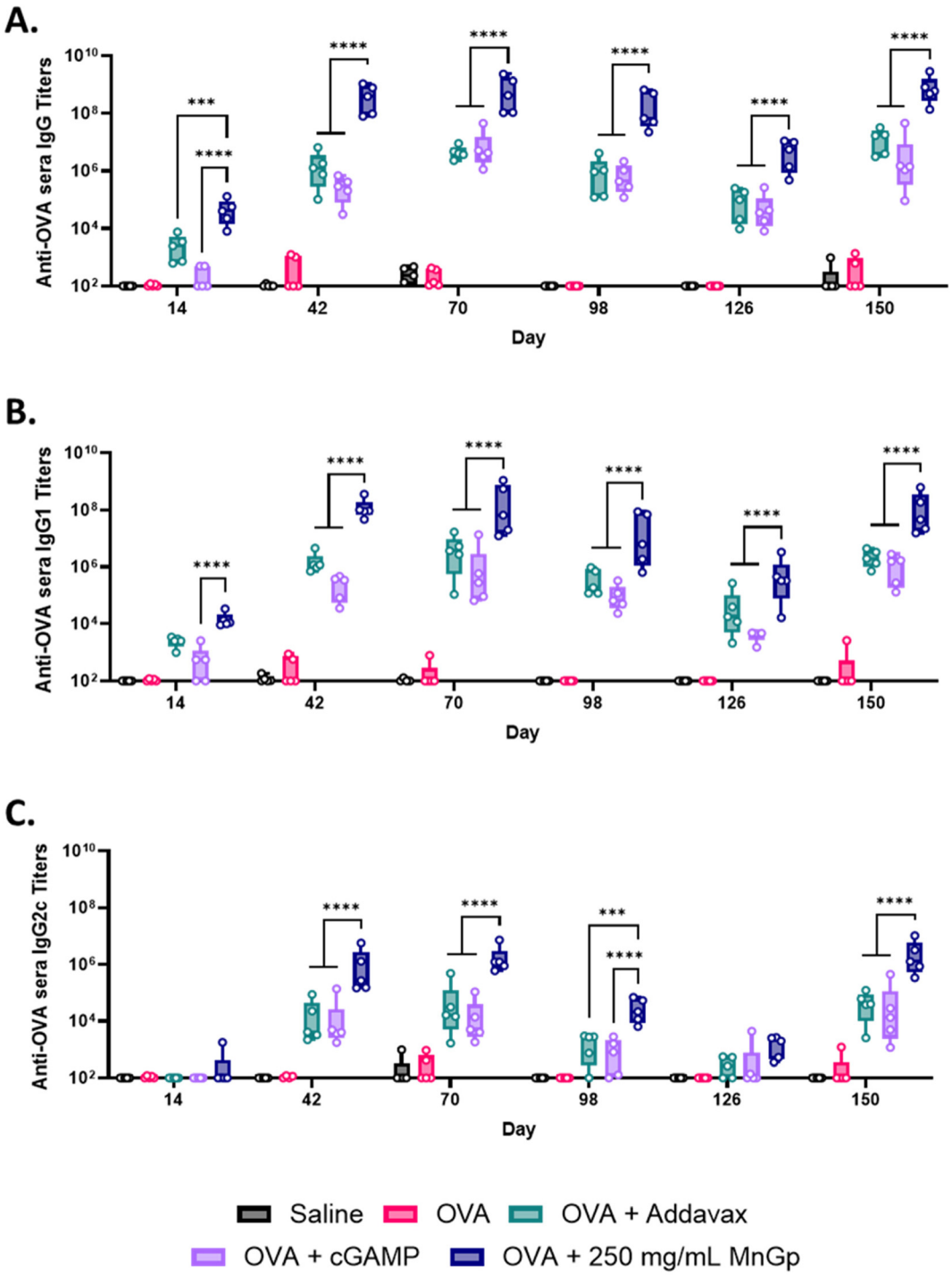

Fig. 4 OVA-specific serum antibody titers following prime-boost-boost immunization schedule. C57BL/6 mice (n = 5) were immunized intramuscularly on days 0, 28, and 140 with saline, unadjuvanted OVA, OVA + Addavax, OVA + cGAMP, or OVA + 250 mg mL^{-1} MnGp. Sera were collected at the indicated timepoints and assessed for OVA-specific (A) total IgG, (B) IgG1 and (C) IgG2c titers *via* ELISA. Data is presented as median ± range. Statistical significance is presented as *p < 0.05, **p < 0.01, ***p < 0.001, and ****p < 0.0001 for an ordinary two-way ANOVA with Tukey's multiple comparisons test. Absence of statistical symbols indicates non-significant differences.

of mice vaccinated with MnGp (Fig. S8A and B). IFN-γ and IL-2 are integral cytokines in T cell responses; particularly, Th1-like responses, driving antigen presenting cell (APC) activation, Th1 differentiation, and T cell proliferation.[66] Therefore, the splenocyte restimulation data indicates that the 250 mg mL^{-1} MnGp gel is an ideal formulation for eliciting Th1 responses compared to more conventional adjuvant systems, consistent with the IgG2c responses (Fig. 3C and 4C).

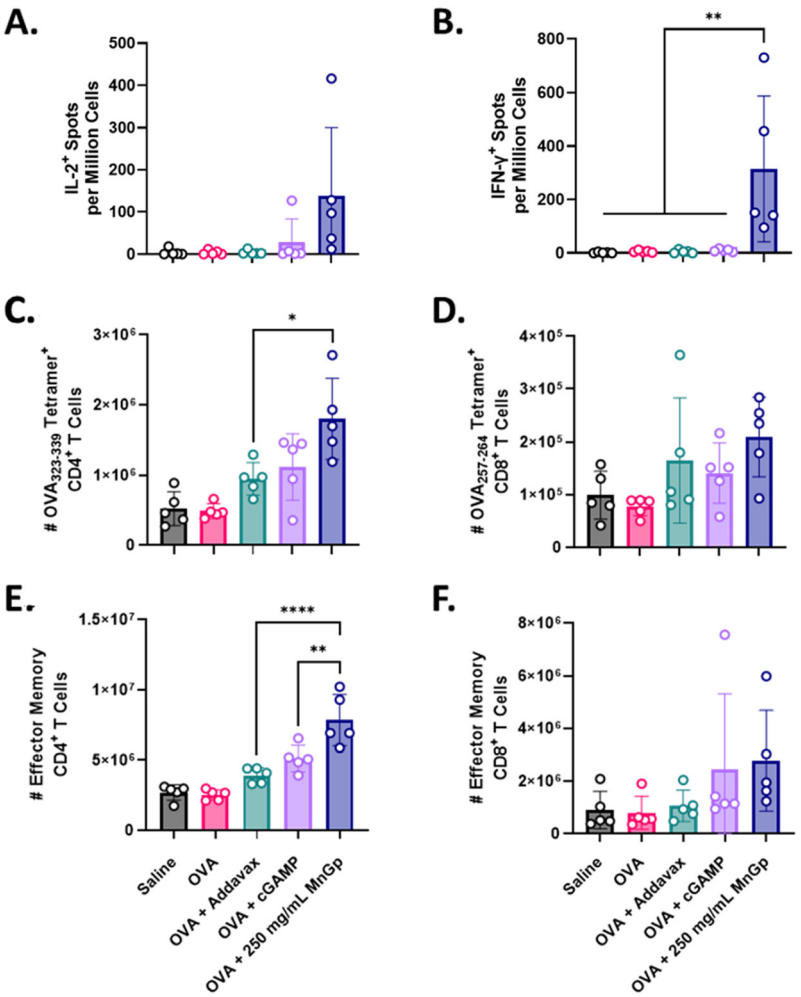

Fig. 5 Antigen recall of splenocytes following a prime-boost-boost immunization schedule. C57BL/6 mice (n = 5) were immunized intramuscularly on days 0, 28, and 140 with saline, unadjuvanted OVA, OVA + Addavax, OVA + cGAMP, or OVA + 250 mg mL^{-1} MnGp. On day 151, splenocytes were collected and re-stimulated with OVA for 36 hours. ELISPOTs were performed to measure (A) IL-2-secreting cells and (B) IFN-γ-secreting cells. Flow cytometry was performed to quantify (C) OVA-specific CD4$^+$ T cells, (D) OVA-specific CD8$^+$ T cells, (E) effector memory CD4$^+$ T cells (CD4$^+$CD44$^+$CD62L$^-$) and (F) effector memory CD8$^+$ T cells (CD4$^+$CD44$^+$CD62L$^-$). Data is presented as mean ± standard deviation. Statistical significance is presented as *p < 0.05, **p < 0.01, and ****p < 0.0001 for ordinary two-way ANOVA with Tukey's multiple comparisons test. Absence of statistical symbols indicates non-significant differences.

When analyzed by flow cytometry, mice immunized with MnGp exhibited elevated OVA-specific CD4$^+$ and CD8$^+$ T cells in spleen with the OVA-specific CD4$^+$ T cell counts significantly higher than those in mice immunized with AddaVax (Fig. 5C and D). The evaluation of the memory phenotype of T cells showed significantly higher effector memory (CD44$^+$CD62L$^-$) CD4$^+$ T cells in the spleen of mice immunized with MnGp compared to mice immunized with AddaVax or cGAMP, however the number of effector memory CD8$^+$ T cells remained similar between them (Fig. 5E and F). Together, these data likely explain the previous IFN-γ and IL-2 ELISPOT and ELISA data (Fig. 5), as effector memory CD4$^+$ T cells are primarily responsible for rapid mobilization of the immune response upon exposure to their cognate antigen.[67] On the other hand, the number of central memory CD4$^+$ and CD8$^+$ T cells (CD44$^+$CD62L$^+$) were similar to our Addavax or cGAMP controls (Fig. S8C and D). In addition to T cells, B cell phenotypes were additionally profiled. Immunization with the 250 mg mL^{-1} MnGp gel induced greater counts of both splenic germinal center (GC; CD19$^+$GL7$^+$CD38$^-$) and activated (CD19$^+$GL7$^-$CD38$^+$) B cells compared to AddaVax and cGAMP, although these differences were not significant (Fig. S9A and B), although there might be a difference if, in the future, we quantify the GC B cells in the draining lymph node of mice immunized with MnGp. Overall, these data align with the properties of the MnGp gel, that compared to AddaVax and cGAMP, the gel forms a highly immunogenic depot that continually releases antigen and Mn, resulting in continuous immune stimulation and maintenance of effector-like phenotypes.

Immunization of MnGp Gel in an aged mice model

To assess the potential of this vaccine platform in immunocompromised populations, we immunized aged mice, a high-risk group with reduced immune responsiveness. We immunized 18 month-old C57BL/6mice (*i.e.* elderly) with MnGp and evaluated the immune response. In this population, the antigen-specific IgG and IgG1 sera titers from mice immunized with MnGp were significantly higher than the titers reached with the Addavax group (Fig. 6A and B). On the other hand, IgG2c titers remained similar in both groups (Fig. 6C). Following antigen recall, splenocytes from aged mice immunized with MnGp showed a non-significant trend toward increased IL-2 production, with similar trends observed for IFN-γ and IL-4. Cytokine levels were generally higher than those in the non-adjuvanted group, but comparable to responses elicited by AddaVax (Fig. 6D, E and Fig. S10).

In general, the immune response induced by MnGp in aged mice was robust, inducing a sustained antigen-specific IgG and IgG1 titers (around 10^6) and detectable T cell responses that indicate the presence of Th1 and Th2 responses in those mice. It is important to highlight that the robust immune response induced by MnGp is a good indicator of the potential of this platform for a high-risk population vaccine, given that other adjuvant systems like cGAMP have only induced IgG titers of the order of around 10^4; in addition, cGAMP induce a practically null presence of IL-2 and IFN-γ cellular responses in aged mice.[49]

Use of MnGp gel for a pox virus vaccine

Mice immunized with MnGp and B5R exhibited high levels of B5R-specific antibody titers for up to 8 weeks post-vaccination. IgG, IgG1 and IgG2c sera titers from mice immunized with MnGp were significantly higher than the titers reached with the Addavax group (Fig. 7A–C), demonstrating the strong immunogenicity induced by this formulation and highlighting the presence of Th1 and Th2 responses *versus* B5R in mice. After the challenge, the immunization with MnGp was the only condition that achieved full (100%) protection *versus* vaccinia virus, where Addavax reached 80% of final survival while the rest of the groups succumbed to infection (Fig. 7D). A similar protection pattern was found after analyzing the weight loss curves and the clinical scores, where in general, a better (but not significant) protection pattern was observed in mice immunized with MnGp compared with Addavax (Fig. S11A and B).

This promising result aligned with the previous immunological characterization, in which we observed a long-lasting antibody response and a strong cellular immune response, suggesting that those mechanisms might be involved in the full protection observed in mice vaccinated with MnGp. In

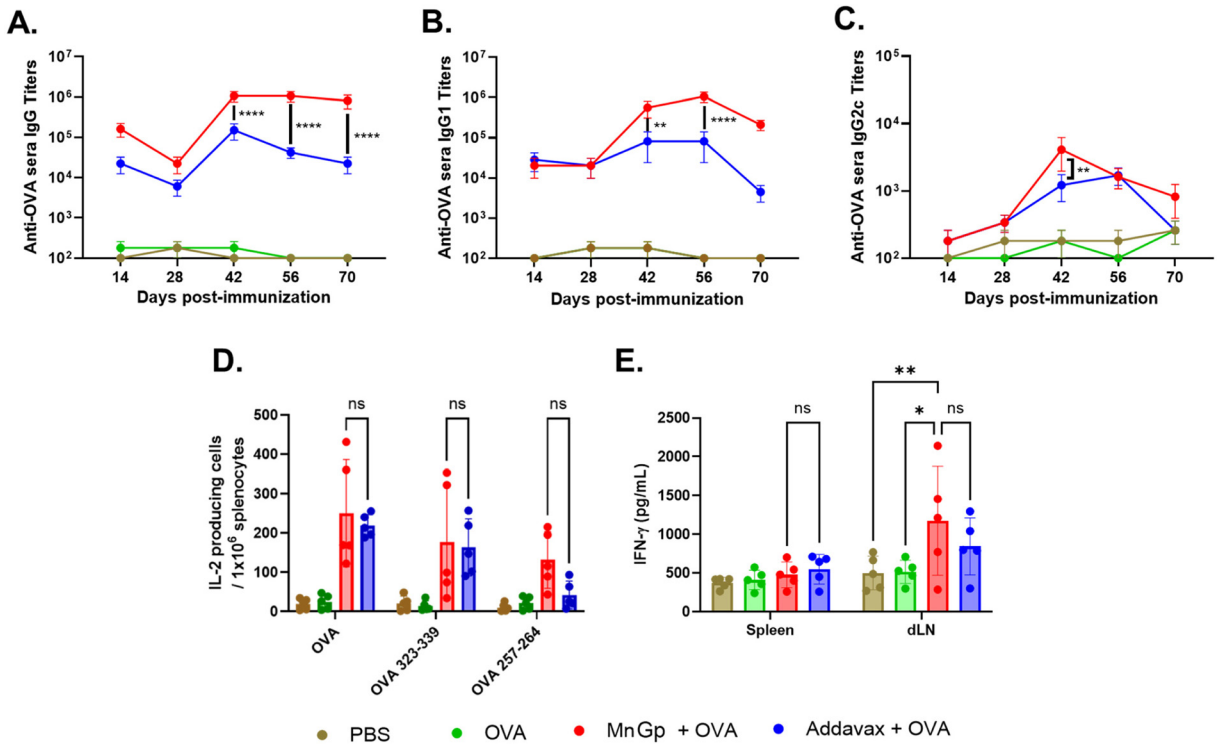

Fig. 6 Humoral and cellular responses in aged mice immunized with MnGp. C57BL/6 18-month-old mice (n = 5) were immunized intramuscularly on days 0, 28 and 77 with PBS, unadjuvanted OVA, MnGp (250 mg mL^{-1}) + OVA or Addavax + OVA. (A) Sera IgG, (B) IgG1 and (C) IgG2c were measured at different timepoints. (D) IL-2 producing cells in spleen and (E) IFN-γ production from splenocytes and dLN cells harvested on day 84 after a re-stimulation with OVA and OVA peptide. Data is presented as mean ± standard deviation. Statistical significance is presented as *p < 0.05, **p < 0.01, and ****p < 0.0001 for an ordinary two-way ANOVA with Tukey's multiple comparisons test.

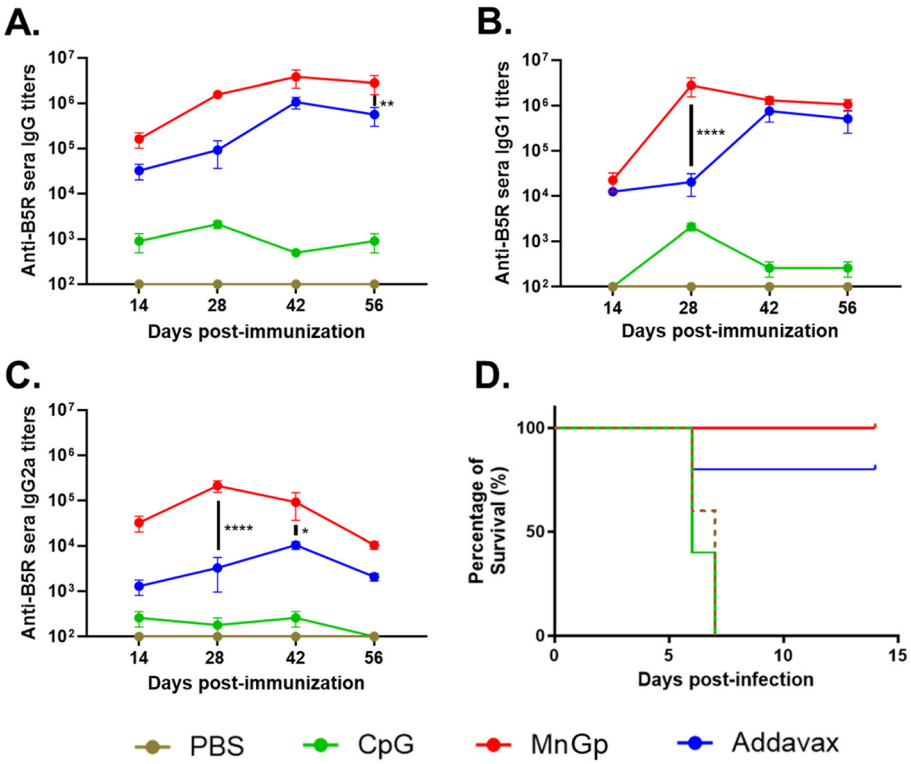

Fig. 7 IgG, IgG1, IgG2a sera titers and survival from mice immunized with MnGp + B5R and challenged with vaccinia virus. BALB/c mice (n = 10) were immunized intramuscularly on days 0 and 28 with PBS, CpG + B5R, MnGp (250 mg mL^{-1}) + B5R or Addavax + B5R. On day 56 the mice were challenged with vaccinia virus. (A) Sera IgG, (B) IgG1 and (C) IgG2a titers at different timepoints. (D) Survival of mice after challenge. Data is presented as mean ± standard deviation. Statistical significance is presented as *p < 0.05, **p < 0.01, and ****p < 0.0001 for an ordinary two-way ANOVA with Tukey's multiple comparisons test.

general, the efficacy of the current FDA-approved monkeypox vaccines is between 75–85%,[68] therefore, would be interesting to keep investigating the potential of MnGp as a vaccine platform against *Orthopox* viruses.

Conclusion

The present work described the synthesis, characterization, and administration of a novel Mn-based gel for vaccine applications. The MnGp gel was fabricated *via* a scalable and facile sonication method, and gels of varying MnGp content displayed tunable release of the model antigen OVA over the course of a week. MnGp exhibited *in vitro* activation of dendritic cells, resulting in elevated type I interferon secretion and increased expression of co-stimulatory markers. Immunization of MnGp with OVA elicited a strong immune response as a single-dose or prime-boost vaccine, showing sustained antibody titers and a robust T cell response, outperforming AddaVax, an analog to the FDA-approved adjuvant MF59. MnGp displayed promising immunological features in aged mice, inducing sustained IgG titers and the presence of specific T cells. Finally, used as a vaccine platform against the *Orthopoxvirus* vaccinia, MnGp was able to produce B5R-specific antibodies and protect all the mice after the viral challenge. Overall, this MnGp platform represents a highly efficacious strategy for improving and prolonging both the humoral and cellular immune responses to subunit vaccines.

Author contributions

J. A. R., M. J. I. and S. A. E. synthesized and characterized the materials. L. O. P., M. J. I., S. A. E., J. A. R., D. D. M., C. T. M., N. R. L., D. A. H., E. S. P., R. N. S. and W. J. P. participated in investigation and data acquisition. M. J. I. primarily curated and organized data. M. J. I., L. O. P. and S. A. E. drafted the original manuscript and figures. All authors participated in manuscript revision. K. M. A. and E. M. B. conceptualized and supervised the research, and K. M. A. secured funding resources.

Conflicts of interest

There are no conflicts to declare. E. M. B., K. M. A., J. A. R., M. J. I., and S. A. E. filed a provisional patent with the University of North Carolina at Chapel Hill (U.S. Provisional Patent Application No. 63/714,626).

Ethical statement

All animal procedures were performed in accordance with the Guidelines for Care and Use of Laboratory Animals of University of North Carolina at Chapel Hill and approved by UNC Institutional Animal Care and Use Committee.

Data availability

The data supporting this study will be available through the NIH NIAID Collaborative Influenza Vaccine Innovation Centers (CIVIC) database. Access can be obtained *via* the database portal, and additional details are available from the corresponding author upon reasonable request.

Supplementary information (SI) is available. See DOI: https://doi.org/10.1039/d5nr03936c.

Acknowledgements

This work was supported, in part, by National Institutes of Health (NIH) NIAID R01AI147497 (PI: Ainslie). This work was performed in part at the Chapel Hill Analytical and Nanofabrication Laboratory, CHANL, a member of the North Carolina Research Triangle Nanotechnology Network, RTNN, which is supported by the National Science Foundation, Grant ECCS-2025064, as part of the National Nanotechnology Coordinated Infrastructure, NNCI. The UNC Flow Cytometry Core Facility (RRID: SCR_019170) is supported in part by P30 CA016086 Cancer Center Core Support Grant to the UNC Lineberger Comprehensive Cancer Center, the North Carolina Biotech Center Institutional Support Grant 2017-IDG-1025, and by the National Institutes of Health 1UM2AI30836-01. Graphics created with BioRender.com. The content is solely the responsibility of the authors and does not necessarily represent the official views of the National Institutes of Health.

References

1 C. M. C. Rodrigues and S. A. Plotkin, Impact of Vaccines; Health, Economic and Social Perspectives, *Front. Microbiol.*, 2020, **11**, 1526.
2 S. W. Roush, T. V. Murphy and Vaccine-Preventable Disease Table Working Group, Historical comparisons of morbidity and mortality for vaccine-preventable diseases in the United States, *J. Am. Med. Assoc.*, 2007, **298**(18), 2155–2163.
3 S. N. Shchelkunov, An increasing danger of zoonotic orthopoxvirus infections, *PLoS Pathog.*, 2013, **9**(12), e1003756.
4 D. Giulio and P. B. Eckburg, Human monkeypox: an emerging zoonosis, *Lancet Infect. Dis.*, 2004, **4**(1), 15–25.
5 M. Keikha, M. Zandhaghighi and S. Shahraki Zahedani, Death-associated with human monkeypox outbreak 2022: the current perspectives - *correspondence*, *Int. J. Surg.*, 2023, **109**(6), 1806–1807.
6 F. M. Lum, *et al.*, Monkeypox: disease epidemiology, host immunity and clinical interventions, *Nat. Rev. Immunol.*, 2022, **22**(10), 597–613.
7 Y. C. Ai-ris, *et al.*, Decline of Mpox Antibody responses after modified vaccinia Ankara–Bavarian Nordic vaccination, *J. Am. Med. Assoc.*, 2024, **332**(19), 1669–1672.
8 S. Chakraborty, *et al.*, Monkeypox vaccines and vaccination strategies: Current knowledge and advances. An update - Correspondence, *Int. J. Surg.*, 2022, **105**, 106869.
9 O. Mitjà, *et al.*, Mpox in people with advanced HIV infection: a global case series, *Lancet*, 2023, **401**(10380), 939–949.
10 B. Ortiz-Saavedra, *et al.*, Epidemiologic situation of HIV and monkeypox coinfection: a systematic review, *Vaccines*, 2023, **11**(2), 246.
11 J. D. Kelly, *et al.*, Incidence of Severe COVID-19 Illness Following Vaccination and Booster With BNT162b2, mRNA-1273, and Ad26.COV2.S Vaccines, *J. Am. Med. Assoc.*, 2022, **328**(14), 1427–1437.
12 D. Y. Lin, *et al.*, Effectiveness of Covid-19 Vaccines over a 9-Month Period in North Carolina, *N. Engl. J. Med.*, 2022, **386**(10), 933–941.
13 F. P. Polack, *et al.*, Safety and Efficacy of the BNT162b2 mRNA Covid-19 Vaccine, *N. Engl. J. Med.*, 2020, **383**(27), 2603–2615.
14 M. N. Uddin and M. A. Roni, Challenges of Storage and Stability of mRNA-Based COVID-19 Vaccines, *Vaccines*, 2021, **9**(9), 1033.
15 N. Sutton, *et al.*, Comparing reactogenicity of COVID-19 vaccines: a systematic review and meta-analysis, *Expert Rev. Vaccines*, 2022, **21**(9), 1301–1318.
16 P. D. Minor, Live attenuated vaccines: Historical successes and current challenges, *Virology*, 2015, **479–480**, 379–392.
17 S. Plotkin, History of vaccination, *Proc. Natl. Acad. Sci. U. S. A.*, 2014, **111**(34), 12283–12287.
18 N. C. Kyriakidis, *et al.*, SARS-CoV-2 vaccines strategies: a comprehensive review of phase 3 candidates, *npj Vaccines*, 2021, **6**(1), 28.
19 S. G. Reed, M. T. Orr and C. B. Fox, Key roles of adjuvants in modern vaccines, *Nat. Med.*, 2013, **19**(12), 1597–1608.
20 E. B. Lindblad, Aluminium compounds for use in vaccines, *Immunol. Cell Biol.*, 2004, **82**(5), 497–505.
21 B. Pulendran, P. S. Arunachalam and D. T. O'Hagan, Emerging concepts in the science of vaccine adjuvants, *Nat. Rev. Drug Discovery*, 2021, **20**(6), 454–475.
22 E. Aleebrahim-Dehkordi, *et al.*, T helper type (Th1/Th2) responses to SARS-CoV-2 and influenza A (H1N1) virus: From cytokines produced to immune responses, *Transpl. Immunol.*, 2022, **70**, 101495.
23 K. L. Knutson and M. L. Disis, Tumor antigen-specific T helper cells in cancer immunity and immunotherapy, *Cancer Immunol. Immunother.*, 2005, **54**(8), 721–728.
24 A. M. Didierlaurent, *et al.*, AS04, an aluminum salt- and TLR4 agonist-based adjuvant system, induces a transient localized innate immune response leading to enhanced adaptive immunity, *J. Immunol.*, 2009, **183**(10), 6186–6197.

25 E. J. Ko and S. M. Kang, Immunology and efficacy of MF59-adjuvanted vaccines, *Hum. Vaccin. Immunother.*, 2018, **14**(12), 3041–3045.
26 V. Bechtold, *et al.*, Functional and epigenetic changes in monocytes from adults immunized with an AS01-adjuvanted vaccine, *Sci. Transl. Med.*, 2024, **16**(758), eadl3381.
27 K. A. Martins, S. Bavari and A. M. Salazar, Vaccine adjuvant uses of poly-IC and derivatives, *Expert Rev. Vaccines*, 2015, **14**(3), 447–459.
28 C. Bode, *et al.*, CpG DNA as a vaccine adjuvant, *Expert Rev. Vaccines*, 2011, **10**(4), 499–511.
29 X. D. Li, *et al.*, Pivotal roles of cGAS-cGAMP signaling in antiviral defense and immune adjuvant effects, *Science*, 2013, **341**(6152), 1390–1394.
30 M. Lv, *et al.*, Manganese is critical for antitumor immune responses via cGAS-STING and improves the efficacy of clinical immunotherapy, *Cell Res.*, 2020, **30**(11), 966–979.
31 C. Wang, *et al.*, Manganese Increases the Sensitivity of the cGAS-STING Pathway for Double-Stranded DNA and Is Required for the Host Defense against DNA Viruses, *Immunity*, 2018, **48**(4), 675–687.
32 R. Zhang, *et al.*, Manganese salts function as potent adjuvants, *Cell. Mol. Immunol.*, 2021, **18**(5), 1222–1234.
33 Z. Zhao, *et al.*, Mn(2+) Directly Activates cGAS and Structural Analysis Suggests Mn(2+) Induces a Noncanonical Catalytic Synthesis of 2′3′-cGAMP, *Cell Rep.*, 2020, **32**(7), 108053.
34 K. P. Hopfner and V. Hornung, Molecular mechanisms and cellular functions of cGAS-STING signalling, *Nat. Rev. Mol. Cell Biol.*, 2020, **21**(9), 501–521.
35 N. Fan, *et al.*, Manganese-coordinated mRNA vaccines with enhanced mRNA expression and immunogenicity induce robust immune responses against SARS-CoV-2 variants, *Sci. Adv.*, 2022, **8**(51), eabq3500.
36 M. E. Aikins, *et al.*, STING-activating cyclic dinucleotide-manganese nanoparticles evoke robust immunity against acute myeloid leukemia, *J. Controlled Release*, 2024, **368**, 768–779.
37 Z. L. Gao, *et al.*, Orchestrated Cytosolic Delivery of Antigen and Adjuvant by Manganese Ion-Coordinated Nanovaccine for Enhanced Cancer Immunotherapy, *Nano Lett.*, 2023, **23**(5), 1904–1913.
38 L. Hou, *et al.*, Manganese-Based Nanoactivator Optimizes Cancer Immunotherapy via Enhancing Innate Immunity, *ACS Nano*, 2020, **14**(4), 3927–3940.
39 Q. Ma, *et al.*, Manganese-based nanoadjuvants for enhancement of immune effect of DNA vaccines, *Front. Bioeng. Biotechnol.*, 2022, **10**, 1053872.
40 X. OuYang, *et al.*, Manganese-Based Nanoparticle Vaccine for Combating Fatal Bacterial Pneumonia, *Adv. Mater.*, 2023, **35**(51), e2304514.
41 N. Qiao, *et al.*, A MnAl double adjuvant nanovaccine to induce strong humoral and cellular immune responses, *J. Controlled Release*, 2023, **358**, 190–203.
42 S. Awate, L. A. Babiuk and G. Mutwiri, Mechanisms of action of adjuvants, *Front. Immunol.*, 2013, **4**, 114.
43 J. Li and D. J. Mooney, Designing hydrogels for controlled drug delivery, *Nat. Rev. Mater.*, 2016, **1**(12), 16071.
44 J. A. Roque 3rd, *et al.*, Enhancement of subunit vaccine delivery with zinc-carnosine coordination polymer through the addition of mannan, *Int. J. Pharm.*, 2024, **656**, 124076.
45 M. B. Lutz, *et al.*, An advanced culture method for generating large quantities of highly pure dendritic cells from mouse bone marrow, *J. Immunol. Methods*, 1999, **223**(1), 77–92.
46 D. Jin and J. Sprent, GM-CSF Culture Revisited: Preparation of Bulk Populations of Highly Pure Dendritic Cells from Mouse Bone Marrow, *J. Immunol.*, 2018, **201**(10), 3129–3139.
47 C. J. Batty, *et al.*, Vinyl Sulfone-functionalized Acetalated Dextran Microparticles as a Subunit Broadly Acting Influenza Vaccine, *AAPS J.*, 2023, **25**(1), 22.
48 S. N. Shchelkunov, *et al.*, Adaptive Immune Response to Vaccinia Virus LIVP Infection of BALB/c Mice and Protection against Lethal Reinfection with Cowpox Virus, *Viruses*, 2021, **13**(8), 1631.
49 D. A. Hendy, *et al.*, Immunogenicity of an adjuvanted broadly active influenza vaccine in immunocompromised and diverse populations, *Bioeng. Transl. Med.*, 2024, **9**(2), e10634.
50 M. Eckshtain-Levi, *et al.*, Metal-Organic Coordination Polymer for Delivery of a Subunit Broadly Acting Influenza Vaccine, *ACS Appl. Mater. Interfaces*, 2022, **14**(25), 28548–28558.
51 A. Frey, J. D. Canzio and D. Zurakowski, A statistically defined endpoint titer determination method for immunoassays, *J. Immunol. Methods*, 1998, **221**(1–2), 35–41.
52 W. Zhang, *et al.*, The use of injectable sonication-induced silk hydrogel for VEGF(165) and BMP-2 delivery for elevation of the maxillary sinus floor, *Biomaterials*, 2011, **32**(35), 9415–9424.
53 X. Wang, *et al.*, Sonication-induced gelation of silk fibroin for cell encapsulation, *Biomaterials*, 2008, **29**(8), 1054–1064.
54 A. Pramanik, *et al.*, Sonication-Induced, Solvent-Selective Gelation of a 1,8-Napthalimide-Conjugated Amide: Structural Insights and Pollutant Removal Applications, *ACS Omega*, 2021, **6**(48), 32722–32729.
55 J. Tong, *et al.*, Physically crosslinked chitosan/alphabeta-glycerophosphate hydrogels enhanced by surface-modified cyclodextrin: An efficient strategy for controlled drug release, *Int. J. Biol. Macromol.*, 2024, **283**(Pt 1), 137163.
56 M. K. Lee, *et al.*, Cryoprotectants for freeze drying of drug nano-suspensions: effect of freezing rate, *J. Pharm. Sci.*, 2009, **98**(12), 4808–4817.
57 M. H. Chen, *et al.*, Methods To Assess Shear-Thinning Hydrogels for Application As Injectable Biomaterials, *ACS Biomater. Sci. Eng.*, 2017, **3**(12), 3146–3160.
58 C. Yan, *et al.*, Injectable solid hydrogel: mechanism of shear-thinning and immediate recovery of injectable beta-hairpin peptide hydrogels, *Soft Matter*, 2010, **6**(20), 5143–5156.

59 L. Wang-Bishop, *et al.*, Potent STING activation stimulates immunogenic cell death to enhance antitumor immunity in neuroblastoma, *J. Immunother. Cancer*, 2020, **8**(1), e000282.
60 F. Sinigaglia, D. D'Ambrosio and L. Rogge, Type I interferons and the Th1/Th2 paradigm, *Dev. Comp. Immunol.*, 1999, **23**(7–8), 657–663.
61 S. Nazeri, *et al.*, Measuring of IgG2c isotype instead of IgG2a in immunized C57BL/6 mice with Plasmodium vivax TRAP as a subunit vaccine candidate in order to correct interpretation of Th1 versus Th2 immune response, *Exp. Parasitol.*, 2020, **216**, 107944.
62 A. M. Collins, IgG subclass co-expression brings harmony to the quartet model of murine IgG function, *Immunol. Cell Biol.*, 2016, **94**(10), 949–954.
63 S. Hauge, *et al.*, Quality and kinetics of the antibody response in mice after three different low-dose influenza virus vaccination strategies, *Clin. Vaccine Immunol.*, 2007, **14**(8), 978–983.
64 M. P. Kunasekaran, *et al.*, Evidence for Residual Immunity to Smallpox After Vaccination and Implications for Re-emergence, *Mil. Med.*, 2019, **184**(11–12), e668–e679.
65 S. N. Gordon, *et al.*, Smallpox vaccine safety is dependent on T cells and not B cells, *J. Infect. Dis.*, 2011, **203**(8), 1043–1053.
66 S. Romagnani, Th1/Th2 cells, *Inflamm. Bowel Dis.*, 1999, **5**(4), 285–294.
67 M. Kunzli and D. Masopust, CD4(+) T cell memory, *Nat. Immunol.*, 2023, **24**(6), 903–914.
68 L. Pischel, *et al.*, Vaccine effectiveness of 3rd generation mpox vaccines against mpox and disease severity: A systematic review and meta-analysis, *Vaccine*, 2024, **42**(25), 126053.